

# Interactions between fractional solitons in bimodal fiber cavities

Tandin Zangmo<sup>1</sup>, Thawatchai Mayteevarunyoo<sup>1</sup>, and Boris A. Malomed<sup>2,3</sup>

<sup>1</sup>*Department of Electrical and Computer Engineering,*

*Faculty of Engineering, Naresuan University, Phitsanulok 65000, Thailand*

<sup>2</sup>*Department of Physical Electronics, School of Electrical Engineering, Faculty of Engineering,  
and the Center for Light-Matter University, Tel Aviv University, Tel Aviv, Israel*

<sup>3</sup>*Instituto de Alta Investigación, Universidad de Tarapacá, Casilla 7D, Arica, Chile*

We introduce a system of fractional nonlinear Schrödinger equations (FNLSEs) which model the copropagation of optical waves carried by different wavelengths or mutually orthogonal circular polarizations in fiber-laser cavities with the effective fractional group-velocity dispersion (FGVD), which were recently made available to the experiment. In the FNLSE system, the FGVD terms are represented by the Riesz derivatives, with the respective Levy index (LI). The FNLSEs, which include the nonlinear self-phase-modulation (SPM) nonlinearity, are coupled by the cross-phase modulation (XPM) terms, and separated by a group-velocity (GV) mismatch (*rapidity*). By means of systematic simulations, we analyze collisions and bound states of solitons in the XPM-coupled system, varying the LI and GV mismatch. Outcomes of collisions between the solitons include rebound, conversion of the colliding single-component solitons into a pair of two-component ones, merger of the solitons into a breather, their mutual passage leading to excitation of intrinsic vibrations, and the elastic interaction. Families of stable two-component soliton bound states are constructed too, featuring a rapidity which is intermediate between those of the two components.

**Keywords:** Fractional nonlinear Schrödinger equations; Riesz fractional derivative; group-velocity dispersion; Kerr nonlinearity; wavelength-division multiplexing; inelastic collisions of solitons; two-component solitons

Dedicated to the memory of Professor David J. Kaup (1939 – 2022)

## I. INTRODUCTION AND THE MODEL

One of many fundamental contributions of David Kaup to mathematical and theoretical physics is the analysis of interactions (alias *crossstalk*) between solitons carried by different channels in wavelength-division-multiplexed (WDM) fiber-optic telecommunication lines [1]. The significance of this problem for applications is well known [2–4], and it is also recognized as a subject of interest to the theory of nonlinear-wave propagation in optical systems in general [5–8].

Recently, the traditional models of the linear and nonlinear propagation of signals in dispersive optical fibers were extended to, and experimentally realized in, fiber cavities with *fractional* group-velocity dispersion (FGVD) [9, 10]. In fact, these works have reported the first experimental realization of the wave propagation in fractional media of any physical nature. The present work, as a contribution to the special issue of Studies in Applied Mathematics dedicated to the memory of David Kaup, aims to extend the analysis of the interaction between solitons in XPM (cross-phase-modulation)-coupled nonlinear channels with FGVD (instead of the ordinary non-fractional GVD). This topic is a basic element of WDM implemented in the fiber cavity (in fact, it is a fiber laser with compensated losses and gain) featuring the effective FGVD. In addition to its significance to the current studies in nonlinear optics, this problem, being closely related to the specific definition of the pseudodifferential operator which represents the fractional derivative (see Eq. (4) below) is directly relevant to other topics covered by Studies in Applied Mathematics.

While fractional derivatives were known for a long time as a formal generalization of the classical calculus [11]–[14], they were introduced in physics by Laskin in the form of fractional quantum mechanics [15, 16] (see also Ref. [17]), which is based on the fractional Schrödinger equation (FSE) for the wave function of particles whose classical motion is performed by random *Lévy flights*. The latter means that the mean distance of a stochastically moving particle from its initial position,  $x = 0$ , grows with time as

$$|x| \sim t^{1/\alpha}, \quad (1)$$

where the *Lévy index* (LI)  $\alpha$  takes values

$$0 < \alpha \leq 2 \quad (2)$$

[18]. In the scaled form, the corresponding FSE for the particle's wave function  $\Psi(x, t)$  is written as

$$i \frac{\partial \Psi}{\partial t} = \frac{1}{2} \left( -\frac{\partial^2}{\partial x^2} \right)^{\alpha/2} \Psi + V(x)\Psi, \quad (3)$$

where  $V(x)$  is the usual external potential. The normal Schrödinger equation corresponds to  $\alpha = 2$ , while in the case of  $\alpha < 2$  the kinetic-energy operator in Eq. (3) is replaced by the Riesz fractional derivative [19], which implies that the fractional differentiation with LI  $\alpha$  is performed by the multiplication of the Fourier transform of the wave function,  $\hat{\Psi}(p)$ , by  $|p|^\alpha$ :

$$\left( -\frac{\partial^2}{\partial x^2} \right)^{\alpha/2} \Psi = \frac{1}{2\pi} \int_{-\infty}^{+\infty} dp |p|^\alpha \int_{-\infty}^{+\infty} d\xi e^{ip(x-\xi)} \Psi(\xi). \quad (4)$$

The fundamental property of Eq. (3) is that a wave packet spreads out in the free space so that its width  $W$  grows with time according to the same equation (1),  $W \sim t^{1/\alpha}$ , i.e., faster than in the usual case corresponding to  $\alpha = 2$ . This conclusion is correlated with the fact that the stochastic Lévy-flight motion, governed by Eq. (1) with  $\alpha < 2$ , is faster than the classical diffusion spread corresponding to  $\alpha = 2$ .

Implementations of the fractional quantum theory were sought for in solid-state setups, including *Lévy crystals* [20] and exciton-polariton condensates in semiconductor microcavities [21]. However, no experimental realization of these proposals has been reported, as yet. An alternative realization of the FSE was proposed by Longhi [22], making use of the commonly known similarity of the quantum-mechanical Schrödinger equation to the parabolic propagation equation for the local amplitude of the classical electromagnetic field under the condition of the paraxial diffraction, replacing time  $t$ , as the evolution variable, by the propagation distance in the waveguide,  $z$  [23]. The so proposed optical  $4f$  (four-focal-lengths) setup refers to a cavity with two lenses and a phase mask placed in the midplane between the lenses. The lenses carry out the direct and inverse Fourier transforms of the light beam with respect to the transverse coordinate in the cavity. The Fourier transform decomposes the beam into parallel-propagating spectral components with transverse wavenumber  $p$ , the distance  $d$  of each component beam from the optical axis being a function of  $p$ . The phase mask is designed so that it imparts a phase shift  $\Delta\phi(d(p))$  to the passing component beam, emulating the phase variation  $\Delta\phi_{\text{frac}}$  which should be produced by the desired fractional diffraction in the Fourier space. According to Eqs. (3) and (4),  $\Delta\phi_{\text{frac}} = \exp(-i|p|^\alpha Z)$ , where  $Z$  is the propagation distance corresponding to the action of the fractional diffraction. Thus, one may emulate the effect of the fractional diffraction, designing the phase mask with  $\Delta\phi(d(p)) = \Delta\phi_{\text{frac}}$ . This setup provides a single-stage (discrete) action of the effective fractional diffraction. One may then approximate the continuous FSE (3), considering many cycles of the light circulation in the cavity, assuming that each cycle gives rise to a small phase shift  $\Delta\phi(d(p))$ . The potential  $V(x)$  in Eq. (3) can be represented by a mirror inserted in the optical cavity [22].

While the effective fractional diffraction, based on the setup outlined above, has not yet been implemented experimentally, the realization of the effective FGVD in fiber cavities was reported recently [9]. It also relies on emulating the action of the FGVD in the Fourier domain by dint of the differential phase shifts imparted to spatially separated spectral-component beams. The phase shifts were imposed by an appropriately designed phase mask, which was created as a computer-generated hologram. Thus, the temporal optical signal propagating in the fiber was Fourier-decomposed into spatially separated spectral components, that were passed through the hologram and recombined back into the temporal domain.

The realization of the FSE as the propagation equation in optics suggests a natural possibility to add effects of the material nonlinearity, thus replacing FSEs by fractional nonlinear Schrödinger equations (FNLSEs). This possibility had drawn much interest in studies in the realm of nonlinear optics at the theoretical level. Appropriate numerical methods for the work combining the fractional derivatives, represented by the nonlocal pseudodifferential operators (see Eq. (4)), and local nonlinearities are available [24, 25], which has made it possible to predict many results for solitons in such systems with the cubic [26]-[37], cubic-quintic [38, 39], and quadratic [40] nonlinear terms. Other nonlinear states, such as fractional discrete solitons [41, 42], Airy waves [43] and domain walls [44], were also predicted in the framework of FNLSEs. Many theoretical results for fractional solitons, in both one- and two-dimensional models, are summarized in recent reviews [45, 46].

The first experimental observation of nonlinear effects in a fiber cavity combining the effective FGVD and Kerr (cubic) nonlinearity was reported very recently [10]. These are transitions (bifurcations) between optical pulses with single- and multi-peak spectral shapes.

The present work addresses interactions between solitons in the two-channel FGVD system with a group-velocity (GV) mismatch,  $c$ . The model, which is based on the pair of XPM-coupled FNLSEs, is introduced in Section 2. Systematic results for collisions between solitons are reported in Section 3, where they are summarized by means of a chart in the parameter plane of  $c$  and LI,  $\alpha$  (see Fig. 13 below). Section 4 produces systematic results for families

of stable two-soliton bound states, which exist in spite of the presence of the group-velocity mismatch between the channels. The paper is concluded by Section 5.

## II. THE MODEL

In the scaled form, the system of FNLSEs for amplitudes  $u$  and  $v$  of the copropagating optical fields in the XPM-coupled channels, carried by different wavelengths, is written as

$$i\frac{\partial u}{\partial z} = \frac{1}{2} \left( -\frac{\partial^2}{\partial \tau^2} \right)^{\alpha/2} u + (|u|^2 + 2|v|^2) u, \quad (5)$$

$$i\frac{\partial v}{\partial z} = -ic\frac{\partial v}{\partial \tau} + \frac{1}{2} \left( -\frac{\partial^2}{\partial \tau^2} \right)^{\alpha/2} v + (|v|^2 + 2|u|^2) v, \quad (6)$$

where  $z$  and  $\tau$  are, as usual, the propagation distance and reduced time [47], while  $\alpha$ , as said above, is the LI which determines the FGVD (cf. Eq. (4)). The sign of the FGVD terms in Eqs. (5) and (6) corresponds to the anomalous temporal dispersion, which is the case of major interest in fiber optics [47], and real  $c$  represents the mismatch in the inverse GV between the channels, alias the relative *rapidity*. The relative coefficient 2 in front of the XPM terms, in comparison to the SPM (self-phase-modulation) ones, is another common feature of the light propagation in fibers [47]. Relevant values of LI are

$$1 < \alpha \leq 2, \quad (7)$$

as in the remaining interval,  $0 < \alpha \leq 1$  (see Eq. (2)), the *critical* or *supercritical collapse* takes place (at  $\alpha = 1$  or  $\alpha < 1$ , respectively) [26, 34, 45, 46], making all solitons unstable.

Another realization of the same system of Eqs. (5) and (6) in fiber optics, with the same ratio, XPM : SPM = 2, can be realized by the copropagation of two mutually orthogonal circular polarizations of light carried by the same wavelength. In that case, parameter  $c$  represents the GV birefringence, which may be imposed by the fiber's twist [47].

The system of Eqs. (5) and (6) conserves four dynamical invariants, namely, the energies (norms) of the two components,

$$E_u = \int_{-\infty}^{+\infty} |u(\tau)|^2 d\tau, \quad E_v = \int_{-\infty}^{+\infty} |v(\tau)|^2 d\tau, \quad (8)$$

the total momentum,

$$P = i \int_{-\infty}^{+\infty} (uu_\tau^* + vv_\tau^*) d\tau, \quad (9)$$

and the Hamiltonian

$$H = -\frac{1}{2\pi} \int_{-\infty}^{+\infty} d\tau_1 \int_{-\infty}^{+\infty} d\tau_2 \int_{-\infty}^{+\infty} d\omega |\omega|^\alpha e^{i\omega(\tau_1 - \tau_2)} [u^*(\tau_1) u(\tau_2) + v^*(\tau_1) v(\tau_2)] + ic \int_{-\infty}^{+\infty} d\tau v^* v_\tau - \int_{-\infty}^{+\infty} d\tau \left( \frac{1}{2} |u|^4 + \frac{1}{2} |v|^4 + 2|u|^2 |v|^2 \right). \quad (10)$$

In interval (7), Eqs. (5) and (6) admit stable single-component soliton solutions, *viz.*,

$$u = \exp(ik_u z) U(\tau), \quad v = 0, \quad (11)$$

$$u = 0, \quad v = \exp(ik_v z) V(\tilde{\tau}), \quad \tilde{\tau} \equiv \tau - cz + \tau_0, \quad (12)$$

where  $k_u$  and  $k_v$  are positive propagation constants,  $\tau_0$  is an initial temporal distance between the two solitons, and

functions  $U$  and  $V$ , which may be assumed real, satisfy equations

$$k_u U + \frac{1}{2} \left( -\frac{d^2}{d\tau^2} \right)^{\alpha/2} U + U^3 = 0, \quad (13)$$

$$k_v V + \frac{1}{2} \left( -\frac{d^2}{d\tau^2} \right)^{\alpha/2} V + V^3 = 0. \quad (14)$$

In this work, we focus on the case of

$$k_u = k_v \equiv k = 1, \quad (15)$$

when two equations (13) and (14) and the respective solitons are actually identical, while  $k = 1$  may be fixed by scaling. Indeed, in WDM systems solitons with equal energies are normally launched into different channels [2]-[8].

In the case of the ordinary (non-fractional) GVD, with  $\alpha = 2$ , the commonly known classical soliton solutions for  $k_u = k_v = 1$  are

$$U_{\text{sol}} = \sqrt{2} \text{sech}(\sqrt{2}\tau), V_{\text{sol}} = \sqrt{2} \text{sech}(\sqrt{2}\tilde{\tau}), \quad (16)$$

the energy of each one being  $E_u = E_v = 2\sqrt{2}$ . On the other hand, in the same case of  $\alpha = 2$  but  $c = 0$ , another obvious solution of Eqs. (13) and (14) is the two-component soliton,

$$u = v = \sqrt{\frac{2}{3}} e^{iz} \text{sech}(\sqrt{2}\tau), \quad (17)$$

with energies  $E_u = E_v = 2\sqrt{2}/3$ .

### III. SOLITON-SOLITON COLLISIONS

For values of LI in interval (7), single-component soliton solutions to Eqs. (13) and (14) with  $k_u = k_v = 1$  were found by means of the squared-operator iteration method [48, 49]. These solutions were used as the input for simulations of collisions between the  $u$ - and  $v$ -solitons, with a sufficiently large initial temporal separation  $\tau_0$  between them, in the anticipation of the collision happening at  $z \simeq \tau_0/c$ . The collisions were simulated by means of the split-step algorithm, separating, at each step  $\Delta z = 10^{-5} \div 10^{-4}$  of marching forward in  $z$ , increments to the solution generated by the linear and nonlinear terms in Eqs. (5) and (6). To handle the linear terms, the discrete Fourier transform was used for calculating  $(-\partial^2/\partial\tau^2)^{\alpha/2}$ . Typically, the initial separation between the solitons was taken as  $\tau_0 = 8$ , which is large enough in comparison with the soliton's temporal width, that may be estimated as  $W \sim (2k)^{-1/\alpha}$ , pursuant to Eqs. (13) and (14) (hence, for  $k = 1$  and  $\alpha \leq 2$ ,  $W$  takes values  $\lesssim 1/\sqrt{2} \approx 0.7$ ). In most cases, the simulations were performed in the domain of size  $|\tau| \leq 128$ , which was represented by a grid composed of 4096 points. This size was sufficient to unequivocally identify outcomes of the collisions. The periodic boundary condition were used in the simulations of the evolution. The accuracy of the simulations was confirmed by monitoring the conservation of energies (8) and momentum (9) (not shown in detail here).

#### A. Collisions in the system with non-fractional GVD ( $\alpha = 2$ )

First, for comparison with results produced by the FGVD system of Eqs. (5) and (6) with  $\alpha < 2$ , we reproduce some known results for soliton-soliton collisions in the system with the ordinary (non-fractional) GVD, which corresponds to  $\alpha = 2$ . Generally, collisions between solitons in that system are inelastic for smaller values of  $|c|$ , and quasi-elastic for larger  $|c|$  [50]. The simulations of Eqs. (5) and (6) with the GV mismatch  $|c| \lesssim 1$  demonstrate an inelastic outcome in Fig. 1 (for  $c = -1$ ), *viz.*, the formation of a pair of two-component solitons, with unequal energies of the components. The emerging compound solitons keep approximately the same rapidities (0 or  $c$ ) which their dominant components had before the collision. This outcome is also called “splitting”, with the implication that each original single-component soliton *splits* in two fragments, which recombine into the pair of two-component solitons. At larger  $|c|$ , Fig. 2 demonstrates a nearly elastic collision for  $c = -2$ . In this case, the  $u$ - and  $v$ -solitons pass through each other, each capturing a barely visible  $v$ - or  $u$ -components, respectively. As shown below in Fig. 13, in the case of  $\alpha = 2$  the collision becomes completely elastic at  $|c| \geq 2.6$ .



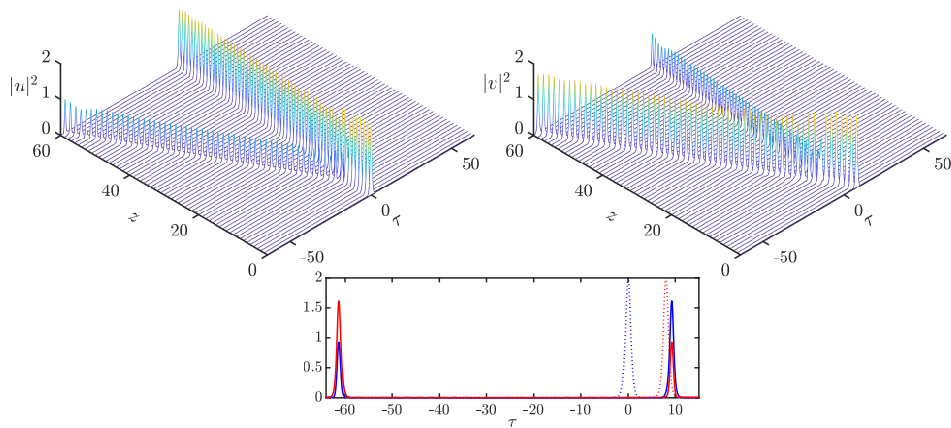


FIG. 1. The inelastic collision between the  $u$ - and  $v$ -component solitons with the GV mismatch  $c = -1$ , produced by simulations of Eqs. (5) and (6) with  $\alpha = 2$  (the ordinary non-fractional, GVD). The collision leads to the formation of a pair of two-component solitons, which keep approximately the same rapidities, 0 and  $c$ , as the single-component solitons had prior to the collision.

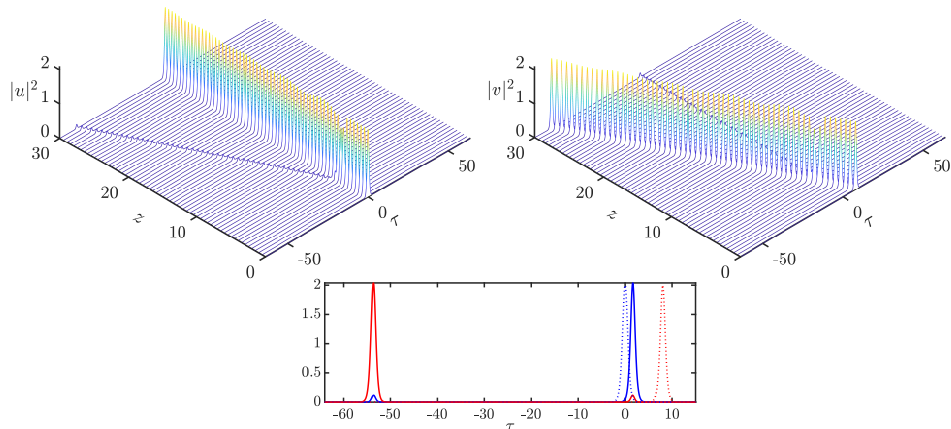


FIG. 2. The same as in Fig. 1, but for  $c = -2.0$ . In this case, the collision is nearly elastic.

### B. Collisions in the system with modern fractionality of the GVD, $\alpha = 1.5$

In the case of a moderate degree of the fractionality, corresponding, typically, to the LI value of  $\alpha = 1.5$ , the collisions with relatively small values of  $|c|$ , such as  $c = -0.3$ , give rise to the outcome identified above as “splitting”, i.e., conversion of the colliding single-component solitons into a pair of compounds with unequal components, as shown in Fig. 3. Also similar to the above-mentioned example, the rapidities of the emerging compound solitons remain very close to those of their dominant “parent” components, i.e., 0 and  $c$ , for the  $u$ - and  $v$ -components, respectively. In addition, the bottom panel in Fig. 3 demonstrates that the collision gives rise to a shift of each soliton as a whole, which is a well-known feature of soliton-soliton interactions [47, 49]. For instance, the center of the soliton with zero rapidity shifts from the initial position,  $\tau_{\text{initial}} = 0$ , to the final one,  $\tau_{\text{final}} \simeq 3$ .

The increase of the rapidity from  $c = -0.3$ , corresponding to Fig. 3, to  $c = -0.5$  leads to the *complete merger* of the colliding solitons into a bound state, as shown in Fig. 4. It is seen that the merger proceeds via the fission and final fusion of the emerging bound state. It appears in the form of a *breather*, with strong internal vibrations. In agreement with the momentum conservation (see Eq. (9)), the bound state moves with rapidity  $\simeq c/2$ , which is the mean value of the rapidities of the original solitons which merge into the bound state.

The merger of the colliding solitons takes place in a narrow interval of values of the GV mismatch  $c$  (see Fig. 13 below). As shown in Fig. 5, the increase of  $|c|$  from 0.5, which corresponds to Fig. 4, to  $c = -0.6$  switches the outcome into the “splitting” regime, which is relatively close to the elastic one, i.e., featuring a pair of compound solitons with a small  $v$ -component attached to the large  $u$ -component, and vice versa, the rapidities staying close to the “parent” values, i.e., 0 and  $c$ , respectively (cf. the outcome displayed in Fig. 2 for  $\alpha = 2$  and  $c = -1$ ). This collision regime is observed, for  $\alpha = 1.5$ , in two intervals of the rapidity, *viz.*,  $-0.9 \leq c \leq -0.6$  and  $-1.8 \leq c \leq -1.1$ .

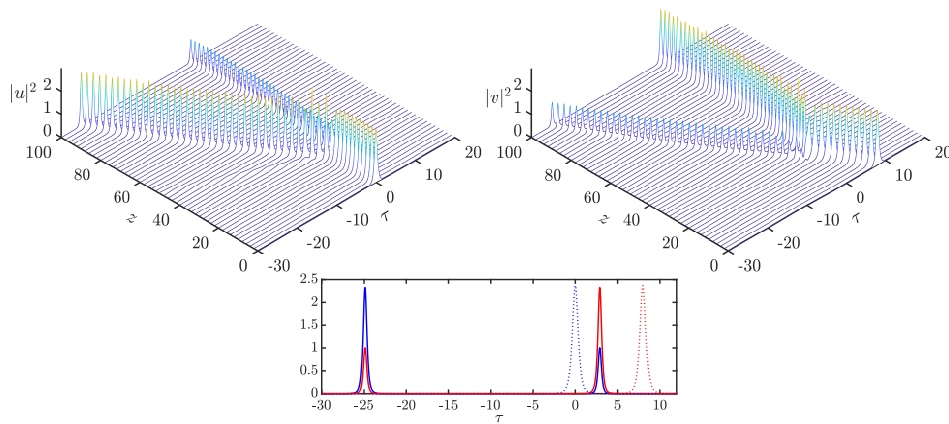


FIG. 3. Top panels: the collision between the  $u$ - and  $v$ -solitons with  $c = -0.3$ , as produced by the simulations of Eqs. (5) and (6) with  $\alpha = 1.5$ . The bottom panel: the soliton profiles,  $|u(\tau)|^2$  and  $|v(\tau)|^2$ , at the input,  $z = 0$  (dotted lines), and in the final configuration (solid lines). This collision can be categorized as “splitting”, similar to the one displayed, for  $\alpha = 2$ , in Fig. 1.

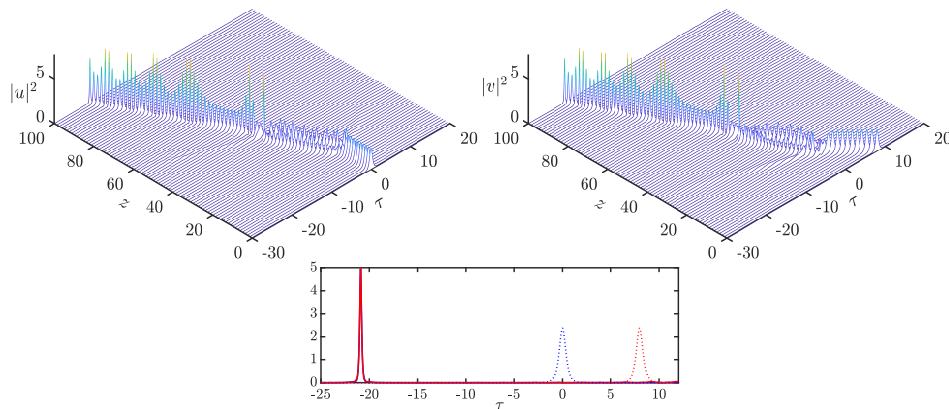


FIG. 4. Top panels: the merger of the colliding solitons into a breather with strong internal vibrations, in the case of  $\alpha = 1.5$  and  $c = -0.5$ . The bottom panel: the soliton profiles,  $|u(\tau)|^2$  and  $|v(\tau)|^2$ , at the input,  $z = 0$  (dotted lines), and in the final configuration (solid lines, which completely overlap for both components).

In the narrow gap between them, the “splitting” outcome is different. As shown in Fig. 6 for  $c = -1.0$ , this case gives rise to the creation of a pair of compound solitons with nearly equal energies of both components. The rapidities of the compound states are seen to be very close to the initial values, i.e., 0 for one compound, and  $c$  for the other. Finally, in the case of  $\alpha = 1.5$  the collisions are completely elastic at  $c > |1.8|$ .

### C. Collisions in the systems with strong fractionality, $\alpha = 1.2$ and 1.1

The system with stronger fractionality – in particular, with  $\alpha = 1.2$ , which is relatively close to the left edge of interval (7) of the admitted values of LI, features different outcomes of the collisions. First, at relatively small values of  $|c|$  the collision seems elastic, but not in the same sense as above: as shown in Fig. 7 for  $c = -0.2$ , the solitons interact with strong repulsion, bouncing back from each other, similar to the collision of hard mechanical particles. Thus, the solitons approximately exchange their velocities, so that the  $u$ -soliton, which originally had rapidity 0, is set in motion with rapidity close to but smaller than  $c$ , while the  $v$ -soliton features a strong drop of the rapidity from the initial value,  $c$ . This outcome occurs in the interval of  $|c| < 0.3$ .

In the region of  $|0.3| \leq c \leq |1.2|$ , the collision leads to the outcome which was defined above as “splitting”, i.e., formation of a pair of compound solitons with unequal energies of the components. As shown in Fig. 8 for  $c = -0.7$ , the difference from the “splitting” outcomes displayed above (see Figs. 1, 3, 5, and 6) is that the two-component solitons are generated in the form of *breathers*, featuring strong internal vibrations. The rapidities of the two breathers take close values, both being intermediate between the initial ones, 0 and  $c$ .

In the adjacent interval,  $|1.3| < c \leq |3.0|$ , Fig. 9 demonstrates (for  $c = -2.0$ ) that the collisions are, generally

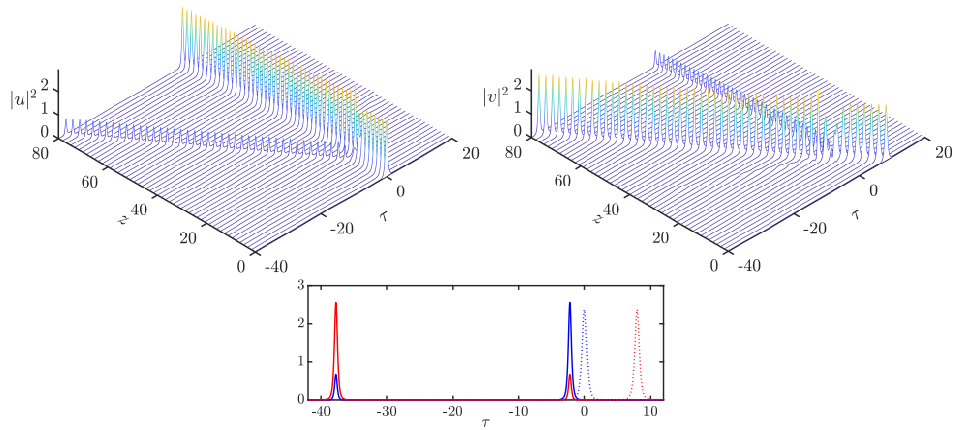


FIG. 5. Top panels: the nearly elastic “splitting” of the colliding solitons, i.e., the generation of two-component solitons, with a small  $v$ -component in one, and a small  $u$ -component in the other, in the case of  $\alpha = 1.5$  and  $c = -0.6$ . The bottom panel: the soliton profiles,  $|u(\tau)|^2$  and  $|v(\tau)|^2$ , at the input,  $z = 0$  (dotted lines), and in the final configuration (solid lines).

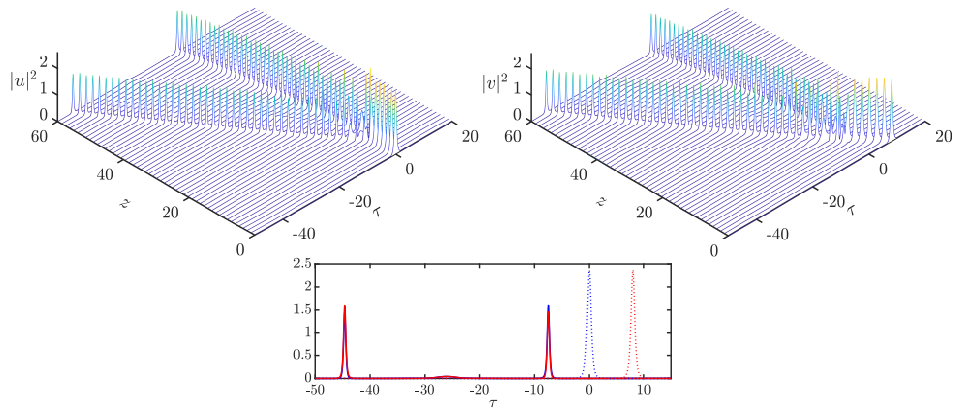


FIG. 6. Top panels: the special case of the “splitting”, namely, the transformation of the colliding solitons into a pair of compound ones, each with nearly equal energies of both components, in the case of  $\alpha = 1.5$  and  $c = -1.0$ . The bottom panel: the soliton profiles,  $|u(\tau)|^2$  and  $|v(\tau)|^2$ , at the input,  $z = 0$  (dotted lines), and in the final configuration (solid lines, which completely overlap for both components in each compound soliton).

speaking, quasi-elastic, but with a peculiarity: after the mutual passage, the solitons develop intrinsic low-amplitude excitations. Finally, at  $|c| > 3$ , the simulations of Eqs. (5) and (6) with  $\alpha = 1.2$  produce completely elastic collisions.

The decrease of LI from  $\alpha = 1.2$  to  $\alpha = 1.1$ , i.e., moving essentially closer to the left edge of interval (7), leads to drastic changes in outcomes of the collisions. In particular, the “splitting” now produces not two, but three solitons, all featuring strong intrinsic vibrations (breathers), as shown in Fig. 10 for  $c = -1.1$ . With the further increase of the rapidity, the “splitting” degenerates into nearly full destruction of the colliding solitons, see Fig. 11 for  $c = -1.5$ . In the case of  $\alpha = 1.1$ , quasi-elastic collisions take place at  $|c| > 1.6$ , featuring the excitation of intrinsic low-frequency vibrations in the solitons, as shown for  $c = -2$  in Fig. 12 (cf. Fig. 9).

#### D. The summary of the results for the soliton-soliton collisions

Outcomes of the collision, produced by systematic simulations of the underlying system of XPM-coupled FNLSEs (5) and (6), are summarized in the parameter plane of LI and GV mismatch,  $(\alpha, c)$ , which is displayed in Fig. 13. In this chart, the “repulsion” outcome, located near the left bottom edge of the parameter plane, implies the rebound of the colliding solitons, see the example in Fig. 7. The “merger”, which takes part in the narrow strip at  $\alpha \leq 1.6$  and  $|c|$  close to 0.5, is exemplified by the picture shown in Fig. 4, in which the colliding solitons merge into a single breather.

The vast area of “splitting” in Fig. 13 includes the cases when the collision converts the single-component solitons

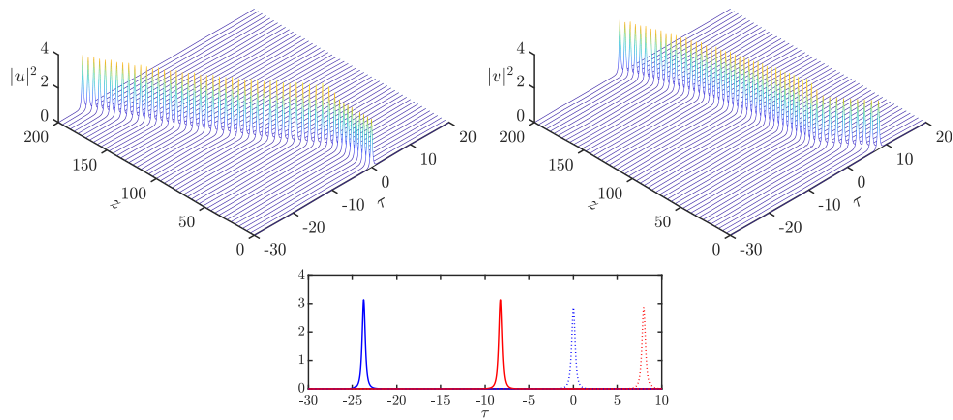


FIG. 7. Top panels: the rebound of the colliding solitons in the case of  $\alpha = 1.2$  and  $c = -0.2$ . The bottom panel: the soliton profiles,  $|u(\tau)|^2$  and  $|v(\tau)|^2$ , at the input,  $z = 0$  (dotted lines), and in the final configuration (solid lines).

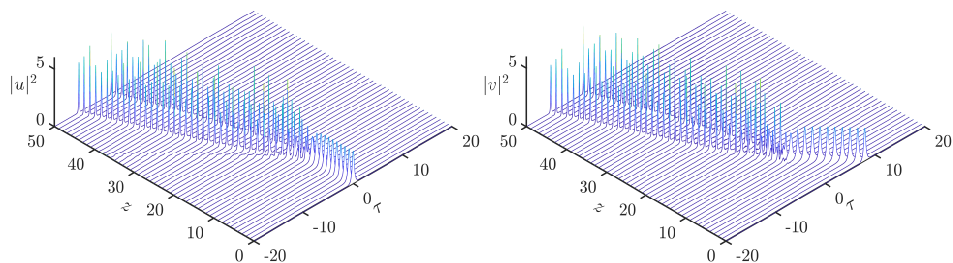


FIG. 8. The “splitting” of the colliding solitons into two-component breathers with close values of the rapidity (intermediate between the initial ones, 0 and  $c$ ), in the case of  $\alpha = 1.2$  and  $c = -0.7$ .

into a pair of two-component ones, such as those displayed in Figs. 1, 3, and 6. Also belonging to this area are outcomes in which the emerging two-component solitons are close to the single-component ones, each featuring one large and one small components (Figs. 2 and 5), and, on the other hand, the cases in which two-component solitons appear in the form of breathers with strong intrinsic vibrations, as in Fig. 8. In addition, the “splitting area” includes a small sub-area (found only for  $\alpha = 1.1$ , i.e., in the case of the strongest fractionality) in which the colliding solitons split in a set of three breathers (Fig. 10) or suffer nearly complete destruction, as in Fig. 11.

The “quasi-elastic” region in Fig. 13 includes the cases when the colliding solitons pass through each other, reappearing in the state with low-frequency intrinsic vibrations, such as in Figs. 9 and 12. Examples of fully elastic collisions, which occur at large values of rapidity  $|c|$  and/or for LI close to the ordinary (non-fractional) value  $\alpha = 2$  (the top right corner in Fig. 13) are not displayed here, as the picture is obvious: the two solitons merely pass through each other, featuring a small shift of their centers, but no changes in their structure or rapidities.

#### IV. TWO-COMPONENT BOUND STATES

The numerical results presented above in Figs. 1, 3, and 6, as well as in Figs. 2 and 5, demonstrate the formation of two-component (compound) solitons, in which the constituents build a robust bound state, in spite of the action of the GV mismatch  $c$ , which tends to split the bound state. In this section, we aim to produce families of such compound solitons directly (not as “accidental” results of the collisions between the single-component solitons), and systematically explore their properties.

Numerical solutions for the bound states were produced by means of a two-stage procedure. First, ansatz

$$u = \exp(ikz)U(\tau), \quad v = \exp(ikz)V(\tau), \quad (18)$$

with  $k = 1$  (as per Eq. (15)), is substituted in the system of XPM-coupled FNLSEs (5) and (6), leading to ordinary

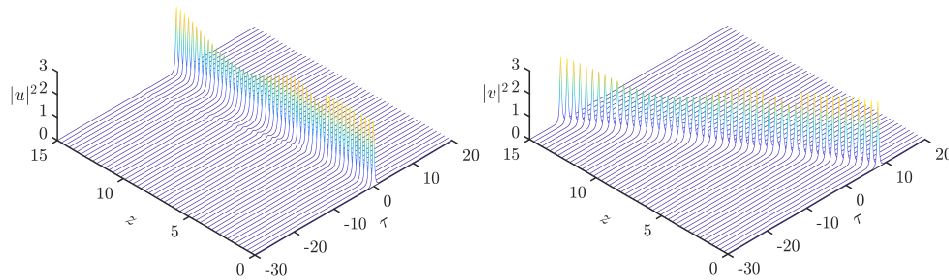


FIG. 9. The quasi-elastic collision of solitons, leading to excitation of low-frequency intrinsic oscillations in them, in the case of  $\alpha = 1.2$  and  $c = -2.0$ .

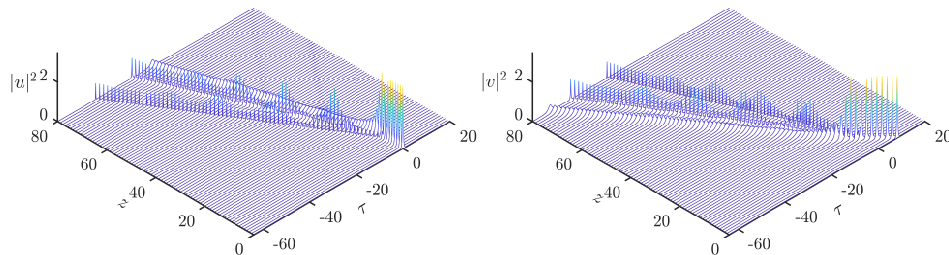


FIG. 10. The collision of solitons in the case of  $\alpha = 1.1$  and  $c = -1.1$ , leading to their “splitting” into a set of three breathers with different rapidities.

differential equations

$$U + \frac{1}{2} \left( -\frac{d^2}{d\tau^2} \right)^{\alpha/2} U + (|U|^2 + 2|V|^2) U = 0, \quad (19)$$

$$V - ic \frac{dV}{d\tau} + \frac{1}{2} \left( -\frac{d^2}{d\tau^2} \right)^{\alpha/2} V + (|V|^2 + 2|U|^2) V = 0, \quad (20)$$

cf. Eqs. (13) and (14). In the absence of the XPM coupling, Eqs. (19) and (20) would produce, severally, single-component solitons such that, if used as initial conditions for the uncoupled equations (5) and (6), would give rise to a quiescent  $u$ -soliton and the  $v$ -soliton moving with rapidity  $c$ .

At the second stage, the two-component solution of Eqs. (19) and (20) was used as the input for the full (XPM-coupled) system of FNLSEs. As a result, the two-component bound state moves with deceleration and slightly varying amplitudes, quickly relaxing towards a stable stationary two-component soliton, with a constant rapidity and constant amplitudes of its components. A typical example of the dynamical relaxation is shown in Fig. 14, for  $\alpha = 1.5$  and  $c = 0.7$ .

The results of the numerical analysis are summarized in Fig. 15, by dint of the dependence of the final rapidity,  $c_{\text{final}}$ , of the established two-component soliton, on the GV mismatch  $c$  in Eqs. (5) and (6), for three different values of LI, *viz.*,  $\alpha = 2, 1.5$ , and  $1.1$ . Naturally,  $c_{\text{final}}$  is smaller than  $c$ , as it is a result of the interplay of the  $u$ - and  $v$ -components, whose proper values of the rapidity are 0 and  $c$ , respectively. For the same three values of LI, additional summary diagrams are provided by Fig. 16, in which the energies and amplitudes of both components of the established two-component solitons are plotted vs.  $c_{\text{final}}$ .

The curves plotted in Figs. 15 and 16 terminate at points where the amplitude of the  $u$ -component becomes too small. The interval of the rapidities in which the two-component solitons exist shrinks with the decrease of LI, in agreement with the fact that the GVD fractionality destroys the Galilean invariance of Eqs. (5) and (6), thus impeding the creation of moving solitons [45, 46].

## V. CONCLUSION

We have considered the copropagation of optical pulses, carried by different wavelengths or orthogonal circular polarizations of light, in the fiber cavity with the effective FGVD (fractional group-velocity dispersion), which is currently available to experiments. The system is modeled by the XPM (cross-phase-modulation)-coupled system of



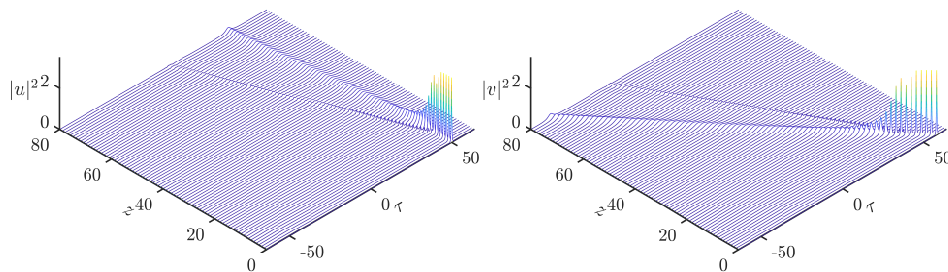


FIG. 11. The collision of solitons in the case of  $\alpha = 1.1$  and  $c = -1.5$ , leading to the extreme form of “splitting”, close to full destruction of the colliding solitons.

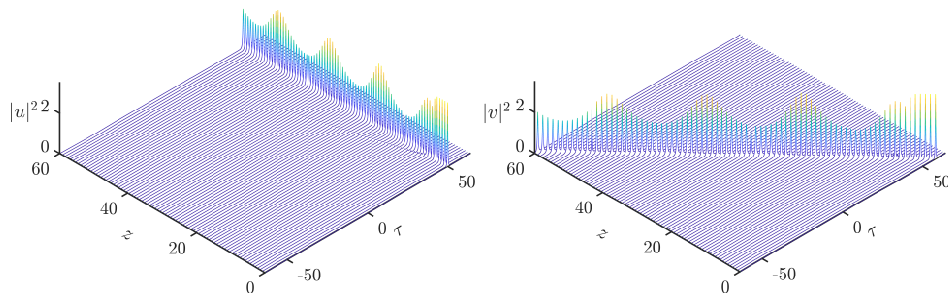


FIG. 12. The quasi-elastic collision of solitons in the case of  $\alpha = 1.1$  and  $c = -2.0$ . The solitons reappear in excited states, featuring low-frequency intrinsic vibrations, with approximately equal frequencies and amplitudes.

FNLSEs (fractional nonlinear Schrödinger equations), with the FGVD represented by the Riesz fractional derivatives, whose LI (Lévy index),  $\alpha$ , takes values  $1 < \alpha \leq 2$  (the ordinary non-fractional GVD corresponds to  $\alpha = 2$ ). The system includes the SPM (self-phase-modulation) nonlinear terms and the GV (group-velocity) mismatch  $c$ . By means of robust numerical methods, we have identified areas in the plane of  $(\alpha, c)$  for different outcomes of the soliton-soliton collisions: mutual rebound, “splitting”, i.e., the transformation of the colliding single-component solitons into a pair of two-component ones, merger of the solitons into a breather, quasi-elastic passage of the solitons with excitations of intrinsic vibrations in both of them, and fully elastic collisions. Using another numerical procedure, families of two-component solitons are constructed systematically, identifying their rapidity and energies of their components.

As an extension of the analysis, it may be interesting to study in detail internal modes of the single- and two-component solitons, the excitation of which is demonstrated by numerical results reported in this work.

## VI. ACKNOWLEDGMENTS

T.Z. would like to express her gratitude to His Majesty the King of Bhutan and Naresuan University for granting the fully funded Master’s Degree scholarship. The Work of T.M. is supported by Faculty of Engineering, Naresuan University (Grant number R2567E039). The work of B.A.M. is supported, in part, by the Israel Science Foundation through grant No. 1695/22.

- 
- [1] D. J. Kaup, B. A. Malomed, and J. Yang, Inter-channel pulse collision in a WDM system with strong dispersion management. *Opt. Lett.* 1998;23:1600–1602.
  - [2] D. Marcuse, A. R. Chraplyvy, and R. W. Tkach, Effect of fiber nonlinearity on long-distance transmission, *J. Lightwave Tech.* 1991;9:121–128.
  - [3] L. F. Mollenauer, S. G. Evangelides, and J. P. Gordon, Wavelength division multiplexing with solitons in ultra-long distance transmission using lumped amplifiers, *J. Lightwave Tech.* 1991;9:362–367.
  - [4] T. Hirooka and A. Hasegawa, Chirped soliton interaction in strongly dispersion-managed wavelength-division-multiplexing systems, *Opt. Lett.* 1998;23:768–770 .
  - [5] M. J. Ablowitz, G. Biondini, and E. S. Olson, Incomplete collisions of wavelength-division multiplexed dispersion-managed solitons, *J. Opt. Soc. Am. B* 2001;18:577–583.



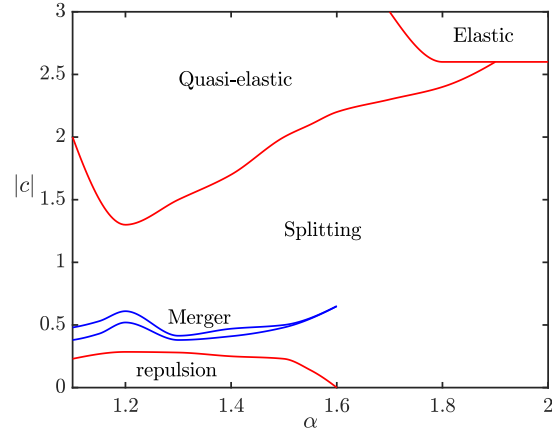


FIG. 13. The chart of outcomes of the soliton-soliton collisions in the plane of LI,  $\alpha$ , and GV mismatch,  $c$ , produced by systematic simulations of Eqs. (5) and (6).

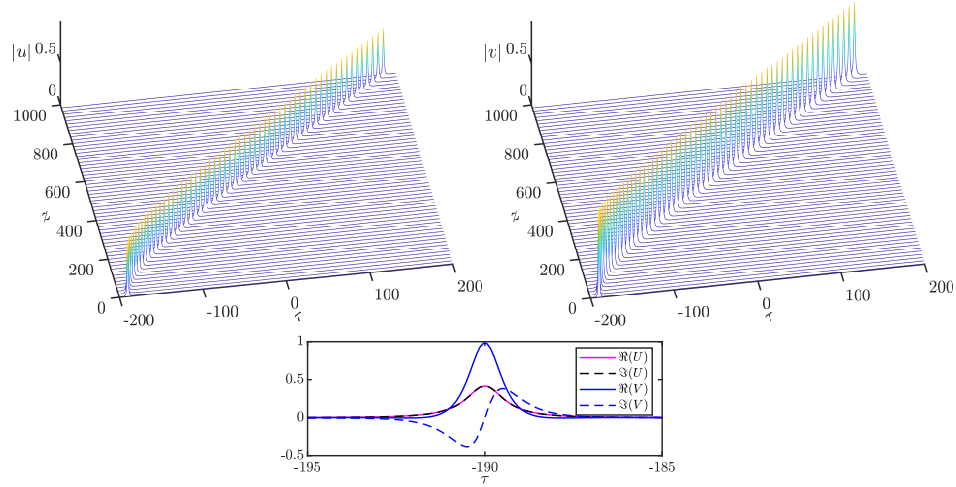


FIG. 14. Left panels: the relaxation of the two-component soliton towards the stationary form, as produced by the numerical simulation of Eqs. (5) and (6), starting from the input produced as a numerical solutions of Eqs. (13) and (14), with  $\alpha = 1.5$  and  $c = 0.7$ . The real and imaginary parts of  $U(\tau)$  and  $V(\tau)$ , used as the input, are displayed in the right panel.

- [6] A. Peleg, M. Chertkov, and I. Gabitov, Interchannel interaction of optical solitons, *Phys. Rev. E.* 2003;68:026605.
- [7] R. Dar, M. Feder, A. Mecozzi, and M. Shtaif, Pulse collision picture of inter-channel nonlinear interference in fiber-optic communications, *J. Lightwave Tech.* 2016;38:593-607.
- [8] S. K. Turitsyn, J. E. Prilepsky, S. T. Le, S. Wahls, L. L. Frumin, M. Kamalian, and S. A. Derevyanko, Nonlinear Fourier transform for optical data processing and transmission: advances and perspectives, *Optica* 2017;4:307-322.
- [9] S. Liu, Y. Zhang, B. A. Malomed, and E. Karimi, Experimental realisations of the fractional Schrödinger equation in the temporal domain, *Nat. Commun.* 2023;14:222.
- [10] S. Liu, Y. Zhang, S. Virally, E. Karimi, B. A. Malomed, and D. V. Seletskiy, Observation of the spectral bifurcation in the Fractional Nonlinear Schrödinger Equation, arXiv:2311.15150.
- [11] N. H. Abel, Opløsning af et Par Opgaver ved Hjælp af bestemte Integraler, *Magazin for Naturvidenskaberne*. Kristiania (Oslo), pp. 55–68 (1823).
- [12] J. Liouville, Mémoire sur quelques questions de géométrie et de mécanique, et sur un nouveau genre de calcul pour résoudre ces questions, *Journal de l'École Polytechnique Paris* **13**, 1–69 (1832).
- [13] M. Caputo, Linear model of dissipation whose Q is almost frequency independent. II, *Geophys. J. Int.* 1967;13:529–539.
- [14] V. V. Uchaikin, *Fractional Derivatives for Physicists and Engineers* (Springer, New York, 2013).
- [15] N. Laskin, Fractional quantum mechanics and Lévy path integrals. *Phys. Lett. A* 2000;268:298–305.
- [16] N. Laskin, *Fractional quantum mechanics* (World Scientific: Singapore, 2018).
- [17] X. Guo and M. Xu, Some physical applications of fractional Schrödinger equation, *J. Math. Phys.* 2006;47:082104.
- [18] B. B. Mandelbrot, *The Fractal Geometry of Nature* (W. H. Freeman, New York, 1982).
- [19] M. Cai and C. P. Li, On Riesz derivative, *Fract. Calc. Appl. Anal.* 2019;22:287–301.

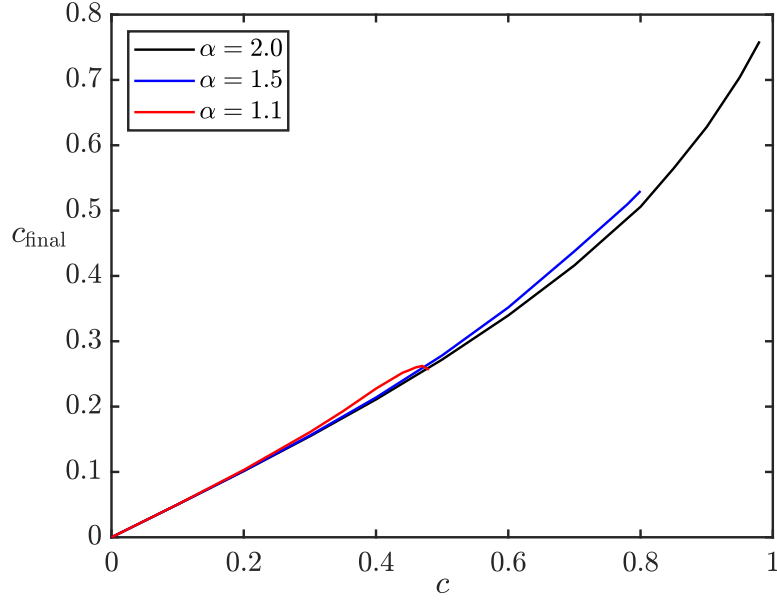


FIG. 15. The final rapidity of the established two-component soliton,  $c_{\text{final}}$ , vs. the GV mismatch parameter  $c$  in the underlying system of Eqs. (5) and (6), for three values of LI,  $\alpha = 2$  (the ordinary non-fractional GVD),  $\alpha = 1.5$  (modern fractionality), and  $\alpha = 1.1$  (strong fractionality).

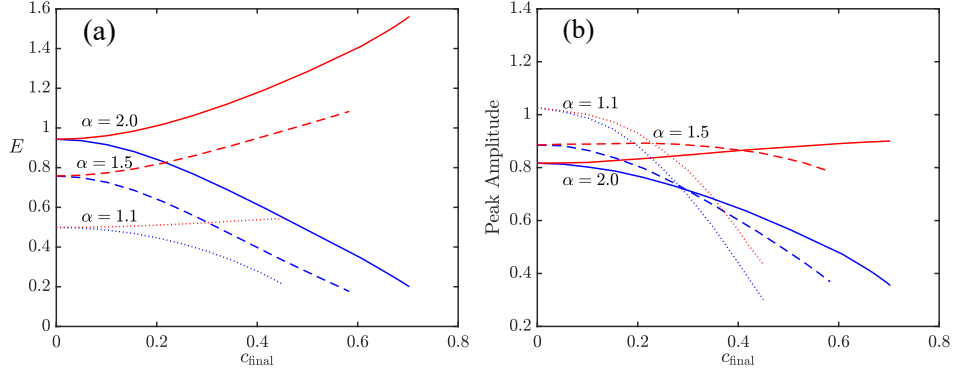


FIG. 16. The energies (a) and amplitudes (b) of the established  $u$ - and  $v$ - components (blue and red curves, respectively) of the compound solitons vs. the their established rapidity,  $c_{\text{final}}$ , for the same LI values as in Fig. 15.

- [20] B. A. Stickler, Potential condensed-matter realization of space-fractional quantum mechanics: The one-dimensional Lévy crystal. *Phys. Rev. E* 2013;88:012120.
- [21] F. Pinski, W. Bao, Y. Zhang, H. Ohadi, A. Dreismann, and J. J. Baumberg, Fractional quantum mechanics in polariton condensates with velocity-dependent mass, *Phys. Rev. B* 2015;92:195310.
- [22] S. Longhi, Fractional Schrödinger equation in optics. *Opt. Lett.* 2015;40:1117–1120.
- [23] Y. S. Kivshar and G. P. Agrawal, *Optical Solitons: From Fibers to Photonic Crystals* (Academic Press, San Diego, 2003).
- [24] S. Secchi and M. Squassina, Soliton dynamics for fractional Schrödinger equations. *Appl. Anal.* 2014;93:1702–1729.
- [25] S. Duo and Y. Zhang, Mass-conservative Fourier spectral methods for solving the fractional nonlinear Schrödinger equation. *Comput. Math. Appl.* 2016;71:2257–2271.
- [26] M. Chen, S. Zeng, D. Lu, W. Hu, and Q. Guo, Optical solitons, self-focusing, and wave collapse in a space-fractional Schrödinger equation with a Kerr-type nonlinearity. *Phys. Rev. E* 2018;98:022211.
- [27] C. Huang and L. Dong, Gap solitons in the nonlinear fractional Schrödinger equation with an optical lattice. *Opt. Lett.* 2016;41:5636–5639.
- [28] J. Xiao, Z. Tian, C. Huang, and L. Dong, Surface gap solitons in a nonlinear fractional Schrödinger equation. *Opt. Express* 2018;26:2650–2658.
- [29] X. K. Yao and X. M. Liu, Solitons in the fractional Schrödinger equation with parity-time-symmetric lattice potential. *Photonics Res.* 2018;6:875–879.

- [30] L. W. Dong and C. M. Huang, Double-hump solitons in fractional dimensions with a  $\mathcal{PT}$ -symmetric potential. *Opt. Exp.* 2018;26:10509–10518.
- [31] S. Arshed, Soliton solutions of fractional complex Ginzburg-Landau equation with Kerr law and non-Kerr law media. *Optik* 2018;160:322–332.
- [32] L. Dong and Z. Tian, Truncated-Bloch-wave solitons in nonlinear fractional periodic systems. *Ann. Phys.* 2019;404:57–64.
- [33] Y. Qiu, B. A. Malomed, D. Mihalache, X. Zhu, X. Peng, and Y. He, Stabilization of single- and multi-peak solitons in the fractional nonlinear Schrödinger equation with a trapping potential. *Chaos Solitons Fract.* 2020;140:110222.
- [34] L. Zeng and J. Zeng, Preventing critical collapse of higher-order solitons by tailoring unconventional optical diffraction and nonlinearities. *Commun. Phys.* 2020;3:26.
- [35] P. Li, B. A. Malomed, and D. Mihalache, Symmetry breaking of spatial Kerr solitons in fractional dimension. *Chaos Solitons Fract.* 2020;132:109602.
- [36] L. Zeng and J. Zeng, Fractional quantum couplers, *Chaos Solitons & Fract.* 2020;140:110271.
- [37] D. V. Strunin and B. A. Malomed, Symmetry-breaking transitions in quiescent and moving solitons in fractional couplers. *Phys. Rev. E* 2023;107:064203.
- [38] P. Li and C. Dai, Double loops and pitchfork symmetry breaking bifurcations of optical solitons in nonlinear fractional Schrödinger equation with competing cubic-quintic nonlinearities. *Ann. Phys. (Berlin)* 2020;532:2000048.
- [39] L. Zeng, D. Mihalache, B. A. Malomed, X. Lu, Y. Cai, Q. Zhu, and J. Li, Families of fundamental and multipole solitons in a cubic-quintic nonlinear lattice in fractional dimension, *Chaos Solitons Fract.* 2021;144:110589.
- [40] L. Zeng, Y. Zhu, B. A. Malomed, D. Mihalache, Q. Wang, H. Long, Y. Cai, X. Lu, and J. Li, Quadratic fractional solitons, *Chaos, Solitons & Fractals* **154**, 111586 (2022).
- [41] M. I. Molina, The fractional discrete nonlinear Schrödinger equation, *Phys. Lett. A* **384**, 126180 (2020).
- [42] H. Almusawa and A. Jhangeer, A Study of the soliton solutions with an intrinsic fractional discrete nonlinear electrical transmission line, *Fractal and Fractional* **6**, 334 (2022).
- [43] L. F. Zhang, X. Zhang, H. Z. Wu, C. X. Li, D. Pierangeli, Y. X. Gao, and D. Y. Fan, Anomalous interaction of Airy beams in the fractional nonlinear Schrödinger equation, *Opt. Exp.* **27**, 27936-27945 (2019).
- [44] S. Kumar, P. Li, and B. A. Malomed, Domain walls in fractional media, *Phys. Rev. E* **106**, 054207 (2022).
- [45] B. A. Malomed, Optical solitons and vortices in fractional media: A mini-review of recent results, *Photonics* **8**, 353 (2021).
- [46] B. A. Malomed, Basic fractional nonlinear-wave models and solitons, *Chaos* **34**, 022102 (2024).
- [47] G. P. Agrawal, *Nonlinear Fiber Optics* (Academic Press, Amsterdam, 2013).
- [48] J. Yang and T. I. Lakoba, Universally-convergent squared-operator iteration methods for solitary waves in general nonlinear wave equations, *Stud. Appl. Math.* **118**, 153-197 (2007).
- [49] J. Yang, *Nonlinear Waves in Integrable and Nonintegrable Systems* (SIAM, Philadelphia, 2010).
- [50] B. A. Malomed and S. Wabnitz, Soliton annihilation and fusion from resonant inelastic collisions in birefringent optical fibers, *Opt. Lett.* **16**, 1388-1390 (1991).